2015

Modulation of photocatalytic properties by strain in 2d BiOBr nanosheets

Haifeng Feng
University of Wollongong, hf533@uowmail.edu.au

Zhongfei Xu
University of Wollongong

Liang Wang
Beihang University

YouXing Yu
Beihang University

David R. G Mitchell
University of Wollongong, dmitchel@uow.edu.au

See next page for additional authors

Publication Details

Feng, H., Xu, Z., Wang, L., Yu, Y., Mitchell, D., Cui, D., Xu, X., Shi, J., Sannomiya, T., Du, Y., Hao, W. & Dou, S. Xue. (2015). Modulation of photocatalytic properties by strain in 2d BiOBr nanosheets. ACS Applied Materials and Interfaces, 7 (50), 27592-27596.

Modulation of photocatalytic properties by strain in 2d BiOBr nanosheets

Abstract
BiOBr nanosheets with highly reactive {001} facets exposed were selectively synthesized by a facile hydrothermal method. The inner strain in the BiOBr nanosheets has been tuned continuously by the pH value. The photocatalytic performance of BiOBr in dye degradation can be manipulated by the strain effect. The low-strain BiOBr nanosheets show improved photocatalytic activity. Density functional calculations suggest that strain can modify the band structure and symmetry in BiOBr. The enhanced photocatalytic activity in low-strain BiOBr nanosheets is due to improved charge separation attributable to a highly dispersive band structure with an indirect band gap.

Keywords
biobr, strain, properties, photocatalytic, modulation, nanosheets, 2d

Disciplines
Engineering | Physical Sciences and Mathematics

Publication Details
Feng, H., Xu, Z., Wang, L., Yu, Y., Mitchell, D., Cui, D., Xu, X., Shi, J., Sannomiya, T., Du, Y., Hao, W. & Dou, S. Xue. (2015). Modulation of photocatalytic properties by strain in 2d BiOBr nanosheets. ACS Applied Materials and Interfaces, 7 (50), 27592-27596.

Authors
Haifeng Feng, Zhongfei Xu, Liang Wang, YouXing Yu, David R. G Mitchell, Dandan Cui, Xun Xu, Ji Shi, Takumi Sannomiya, Yi Du, Weichang Hao, and S X. Dou

Modulation of Photocatalytic Properties by Strain in 2D BiOBr Nanosheets

Haifeng Feng,[†,‡,#] Zhongfei Xu,[†,‡] Liang Wang,[‡] Youxing Yu,[§,#] David Mitchell,[‖] Dandan Cui,[‡] Xun Xu,[†,#] Ji Shi,[⊥] Takumi Sannomiya,[⊥] Yi Du, [*,†,#] Weichang Hao, [*,†,‡,#] Shi Xue Dou[†,#]

[†] Institute for Superconducting and Electronic Materials (ISEM), Australian Institute for Innovative Materials (AIIM), University of Wollongong, Wollongong, NSW 2525, Australia

[‡] Department of Physics and Key Laboratory of Micro-Nano Measurement, Manipulation and Physics, Ministry of Education (MOE), Beihang University, Beijing 100191, China

[§] School of Materials Science and Engineering, Beihang University, Beijing 100191, China

[‖] Electron Microscopy Centre, Australian Institute for Innovative Materials (AIIM), University of Wollongong, Wollongong, NSW 2525, Australia

[⊥] Department of Metallurgy and Ceramics Science, Tokyo Institute of Technology, Tokyo 152-8552, Japan

[#] UOW-BUAA Joint Research Centre, University of Wollongong, Wollongong, NSW 2525, Australia

* Correspondence should be addressed to W. C. H. or Y. D. (email: whao@buaa.edu.cn or yi_du@uow.edu.au).

Abstract

BiOBr nanosheets with highly reactive {001} facets exposed were selectively synthesized by a facile hydrothermal method. The inner strain in the BiOBr nanosheets has been tuned continuously by the pH value. The photocatalytic performance of BiOBr in dye degradation can be manipulated by the strain effect. The low-strain BiOBr nanosheets show improved photocatalytic activity. Density functional calculations suggest that strain can modify the band structure and symmetry in BiOBr. The enhanced photocatalytic activity in low-strain BiOBr

nanosheets is owing to improved charge separation due to a highly dispersive band structure with an indirect band gap.

KEYWORDS: *BiOBr, {001} facets, strain, photocatalysis, density functional calculations*

The ability to continuously control the electronic structures in photocatalysts is highly desirable for a wide range of energy and environmental applications, including H_2 production by water splitting, carbon fixation, and the elimination of pollution.[1,2] For example, the absorption spectrum and the quantum conversion efficiency of a photocatalyst, which determine its performance, can be modulated by tuning the band gap (E_g), the positions of the valence band (VB) and the conduction band (CB), and the band dispersion of photocatalysts.[3] In a similar way to chemical composition, strain is a continuous variable that is capable of altering electronic structure. Although strain engineering is a straightforward method, its potential in photocatalysis remains largely under-exploited.

Bismuth oxyhalides BiOX (X = Cl, Br, I) are *p*-block photocatalysts that have attracted considerable attention due to their unique two-dimensional (2D) layered structure and excellent photocatalytic properties under visible light.[4-9] In BiOX, $[Bi_2O_2]^{2+}$ slabs are interleaved with double halogen atoms slabs by strong electrovalent bonds along the [001] direction, while two closely adjacent slabs of halogen atoms are connected by van de Waals interactions.[10,11] The dispersive VB and CB induced by *sp* hybridization give rise to high mobility of the photo-induced charge carriers. In addition, the internal electric field resulting from the asymmetric charge distribution between $[Bi_2O_2]^{2+}$ and the halogen layers facilitates the effective separation of these photo-induced charge carriers, and hence, enables the photocatalytic activity of BiOX.[12-14] Due to their 2D layered structure, the electronic structure of BiOX compounds is highly

sensitive to even a subtle inner strain variation.[15] It is, however, a practical challenge to modulate the photocatalytic properties through fine-tuning the inner strain in nanoscale BiOX.

In this work, we illustrate experimentally and theoretically that the photocatalytic performance of BiOBr nanosheets can be tuned by the inner strain effect. The characterizations of photocatalytic degradation and geometric phase analysis (GPA) of the transmission electron microscope (TEM) images indicate that the distribution and intensity of the inner strain dominate the photocatalytic activity of BiOBr nanosheets. Density functional theory (DFT) calculations demonstrate that the strain-modulated photocatalytic properties in BiOBr originate from variation of the intrinsic electronic structure of this photocatalyst.

Figure 1a and **1d** shows two typical morphologies of BiOBr nanosheets, square-shaped (BiOBr-1) and circle-shaped BiOBr (BiOBr-4), which were fabricated by hydrothermal reaction with different pH values (also see the Supporting Information for synthesis procedure andthe samples synthesized with the other pH values). We found that the BiOBr nanosheets underwent a morphology transition from square-like to circle-like when the pH value was decreased. The BiOBr nanosheets are several micrometres in size. The thicknesses of the BiOBr-square and BiOBr-circle nanosheets are 31 nm and 22 nm, respectively, as revealed by TEM in **Figure 1b** and **1e**. The insets demonstrate the layered structure of the BiOBr nanosheets. The interlayer distance is approximate 0.8 nm for both samples. As shown in **Figure 1c** and **1f**, the *d*-spacing of 0.27 nm indicates that the (110) face is along the in-plane BiOBr nanosheets. The corresponding insets show the selected area electron diffraction (SAED) patterns, in which the marked spots can be indexed as (200) face, (110) face and (1-10) face. Hence, the exposed surfaces can be identified as {001} facets for both the BiOBr-square and the BiOBr-circle nanosheets.

By carefully examining the XRD patterns, obvious diffraction peak shifts could be identified (**Figure S1** in the Supporting Information). It indicates that the inner strain strength varies with different samples. In order to reveal the details of the morphology dependence of the inner strain, we carried out TEM characterization and GPA simulation based on the HRTEM images, as shown in **Figure 2**.[16-18] The in-plane wrinkles observed in the TEM images of the BiOBr-square nanosheets reflect the existence of a large inner strain, while the BiOBr-circle sample exhibits a relatively strain-free character, as shown in **Figure 2a** and **2c**. **Figure 2b** and **2d** show the inner strain distribution maps of the BiOBr nanosheets in the xy-direction (E_{xy}), the x-direction (E_{xx}), and the y-direction (E_{yy}), respectively, as obtained by strain simulation. The inhomogeneous compressive strain distribution in the BiOBr-square nanosheets is reflected by the severe local lattice distortions across the whole surface in **Figure 2b**. In contrast, the BiOBr-circle nanosheets exhibit a quite uniform strain distribution, and this sample shows much less lattice distortion in the strain maps in **Figure 2d**. It should be noted that the strain difference across the BiOBr-square nanosheets is higher than that across the BiOBr-circle nanosheets. For example, the strain in the BiOBr-square sample varies from 0.73 to 1.29 (E_{xy}), from 0.78 to 1.21 (E_{xx}), and from 0.80 to 1.16 (E_{yy}), while in BiOBr-circle, it varies from 0.88 to 1.17 (E_{xy}), from 0.87 to 1.10 (E_{xx}), and from 0.93 to 1.08 (E_{yy}). These results confirm that the inner strain of the BiOBr nanosheets can be varied by the morphology, which can be precisely tuned by the fabrication conditions (**also see the Supporting Information**).

Figure 3a shows the UV-Vis diffuse reflectance spectra of the BiOBr nanosheets with different strains. It reveals a clear absorption edge at the wavelength of 460 nm for BiOBr-square and 440 nm for BiOBr-circle, which verifies that both BiOBr nanosheets could effectively absorb visible light. The E_g values of BiOBr-square and BiOBr-circle are estimated to be 2.68

eV and 2.82 eV, respectively, as determined by the Tauc formula and shown in the inset of **Figure 3a**. This indicates that the inner strain has a significant effect on the band gap of BiOBr. As shown in **Figure 3b**, the BiOBr samples exhibit excellent photocatalytic performance in rhodamine B (Rh. B) degradation. Their photocatalytic activities are higher than for N-doped P25 TiO_2 nanopowders. The low-strain BiOBr-circle sample shows the highest activity among all the samples, and it demonstrates almost 100 % degradation of Rh. B within 30 min. As demonstrated in **Figure 3c**, the apparent first-order rate constant (*k*) for BiOBr-circle is almost twice those for BiOBr-square and the N-doped P25 TiO_2 nanopowders. Similar results were also observed for degradation of other dyes, such as methyl orange (MO), as shown in **Figure 3d** and **3e**. As shown in **Figure S4**, both the BiOBr-square and the BiOBr-circle samples can degrade phenol under visible light. Again, the BiOBr-circle nanosheets show better visible-light photocatalytic degradation performance on phenol than the BiOBr-square nanosheets. The photocurrent response of the BiOBr samples were measured for several On-Off cycles under visible light irradiation. As shown in **Figure 3f**, the photocurrent of the BiOBr samples exhibits a quick response to light irradiation, with the photocurrent sharply decreasing to zero as soon as the light is turned off, while the photocurrent quickly reaches stable values when the light is turned on. The stable photocurrents measured on the BiOBr-square and BiOBr-circle samples under visible light are 0.7 μA and 1.5 μA, respectively. The higher photocurrent of BiOBr-circle than BiOBr-square under visible light suggests that more efficient photoexcited charge carrier separation and less recombination of electron-hole pairs were possibly achieved by decreasing the inner strain in the BiOBr nanosheets.

We carried out DFT calculations in order to the reveal the strain effect (both compressive and tensile strains) on the electronic structure of BiOBr, which dominates the photocatalytic

properties.[19-21] The strain-free and compressive-strained BiOBr show the typical electronic features of an indirect-band-gap semiconductor. It changes to a direct band-gap semiconductor, however, if tensile strain is present in BiOBr. With a 9.1% tensile strain in the BiOBr lattice, the valence band maximum (VBM) of BiOBr moves from the R point to the Z point, while the conduction band minimum (CBM) is still located at the same high symmetry point (Z point) in *k*-space. It is found that the E_g of BiOBr can be modulated by the strain effect, as shown in **Figure 4a**. For example, the band gap varies between 1.94 eV, 2.12 eV, and 1.27 eV in BiOBr which has 8.8% compressive strain, is free of strain, and has 9.1% tensile strain, respectively. Both compressive and tensile strains lead to a narrowed band gap, which is also observed in the other indirect-band-gap semiconductors.[22] **Figure 4b** shows the calculated density of states (DOS). It is found that the bottom of the CB of strain-free BiOBr is mainly contributed by Bi 6*p*, and the top of the VB is dominated by Br 3*p*, O 2*p*, and Bi 6*s* orbitals. While under tensile strain, the contribution of Bi 6*s* to the VBM is suppressed.

Several key factors can affect the photocatalytic activity of BiOBr nanosheets in photocatalytic reactions, which include photon absorption, separation of photoexcited carriers, and surface area. Our UV-Vis diffuse reflectance spectra results demonstrate that the band gap of BiOBr-square (E_g = 2.68 eV) is smaller than that of BiOBr-circle (E_g = 2.82 eV). BiOBr-square is, therefore, expected to have a broader range of light absorption, in contrast to BiOBr-circle. BET measurements reveal that the BiOBr-square sample exhibits a larger surface area of 7.03 m^3/g compared to BiOBr-circle (4.49 m^3/g) (See Supporting Information). It is interesting, however, that the photocatalytic measurements indicate that the photocatalytic activity of BiOBr-sqaure is much lower than that of BiOBr-circle. This is because the photoexcited charge separation in BiOBr determines the overall photocatalytic activity in the photocatalytic process,

which was also reported in previous works.[23,24] As shown in **Figure 3f**, the photocurrent measurements suggest that the charge separation is indeed more efficient in BiOBr-circle nanosheets than in BiOBr-square nanosheets. Based on the DFT calculation results, we believe that the electronic structure of the BiOBr-circle sample may facilitate the separation of photoexcited charge carriers. It was found that the interactions between Br atoms and $[Bi_2O_2]^{2+}$ slabs mediated by weak van de Waals coupling are tunable by the strain effect. In other words, the band symmetry of BiOBr can be modulated by strain through tuning the electronic interaction between the Br atoms and the $[Bi_2O_2]^{2+}$ slabs. The dramatic changes in the band symmetry, e.g. from direct to indirect band gap or the change of energy dispersion due to the strain, would affect the separation of photoexcited charge carriers. The electron-hole recombination occurring in indirect semiconductors typically requires the emission of multiple phonons to accommodate the energy and momentum differences between the CB and the VB. An appropriate rearrangement of the electronic symmetry, for instance, in the BiOBr-circle sample, may tune the momentum mismatch and improve electron-hole separation. Moreover, the VB and CB in strain-free BiOBr are more dispersive, which is expected to lead to a high mobility of photoexcited charge carriers. In the case of the BiOBr-square nanosheets, their electronic structure modifications by the strain effect might depress the separation of photoexcited charge carriers, and consequently, weaken the photocatalytic performance. In addition, strain also leads to the formation of structural defects in 2D materials. In BiOBr-square nanosheets, a large strain of 1.8 % is verified by the XRD and GPA results (**Figure S1** and **Figure 2**). It is believed that strain-induced defects will act as recombination centres for photoexcited electrons and holes, and also depress the quantum conversion efficiency of strained BiOBr-square nanosheets.

In summary, the strain effect on the photocatalytic activity of BiOBr nanosheets with highly reactive {001} facets exposed was studied. The XRD, TEM, and strain tensor simulation results reveal that the intensity and distribution of inner strain in the BiOBr nanosheets can be modulated by adjusting the pH value in the synthesis reaction. It is found that the strain effect can effectively tune the photocatalytic activity of BiOBr nanosheets in dye degradation. Our work suggests that strain engineering could be an effective approach to controlling the electronic structure of semiconductors for further enhancement of their efficiency in converting light into other forms of energy.

Acknowledgements

This work is supported by the Australian Research Council (ARC) through a Discovery Project (DP 140102581), and by the National Natural Science Foundation of China (Nos. 51472016, 51272015). The authors thank Dr. T. Silver for her valuable comments on this work.

ASSOCIATED CONTENT

Supporting Information Available: Experimental details and supplementary results. This material is available free of charge via the Internet at http://pubs.acs.org.

References

(1) Chen, X.; Liu, L.; Yu, P. Y.; Mao, S. S. Increasing Solar Absorption for Photocatalysis with Black Hydrogenated Titanium Dioxide Nanocrystals. *Science* **2011**, *331*, 746-750.

(2) Zhang, J.; Sun, J.; Maeda, K.; Domen, K.; Liu, P.; Antonietti, M.; Fu, X.; Wang, X. Sulfur-mediated Synthesis of Carbon Nitride: Band-gap Engineering and Improved Functions for Photocatalysis. *Energy Environ. Sci.* **2011**, *4*, 675-678.

(3) Tong, H.; Ouyang, S.; Bi, Y.; Umezawa, N.; Oshikiri, M.; Ye, J. Nano-photocatalytic

Materials: Possibilities and Challenges. *Adv. Mater.* **2012**, *24*, 229-251.

(4) Cheng, H.; Huang, B.; Dai, Y. Engineering BiOX (X = Cl, Br, I) Nanostructures for Highly Efficient Photocatalytic Applications. *Nanoscale* **2014**, *6*, 2009-2026.

(5) Li, J.; Yu, Y.; Zhang, L. Bismuth Oxyhalide Nanomaterials: Layered Structure Meet Photocatalysis. *Nanoscale* **2014**, *6*, 8473-8488.

(6) Ye, L.; Su, Y.; Jin, X.; Xie, H.; Zhang, C. Recent Advances in BiOX (X = Cl, Br, I) Photocatalysts: Synthesis, Modification, Facet Effect and Mechanisms. *Environ. Sci.: Nano* **2014**, *1*, 90-112.

(7) Zhang, H.; Liu, L.; Zhou, Z. Towards Better Photocatalysts: First-principles Studies of the Alloying Effects on the Photocatalytic Activities of Bismuth Oxyhalides under Visible Light. *Phys. Chem. Chem. Phys.* **2012**, *14*, 1286-1292.

(8) Zhang, H.; Liu, L.; Zhou, Z. First-principles Studies on Facet-dependent Photocatalytic Properties of Bismuth Oxyhalides (BiOXs). *RSC Adv.* **2012**, *2*, 9224-9229.

(9) Zhang, H.; Yang, Y.; Zhou, Z.; Zhao, Y.; Liu, L. Enhanced Photocatalytic Properties in BiOBr Nanosheets with Dominantly Exposed (102) Facets. *J. Phys. Chem. C.* **2014**, *118*, 14662-14669.

(10) Deng, H.; Wang, J.; Peng, Q.; Wang, X.; Li, Y. Controlled Hydrothermal Synthesis of Bismuth Oxyhalide Nanobelts and Nanotubes. *Chem. Eur. J.* **2005**, *11*, 6519-6524.

(11) An, H.; Du, Y.; Wang, T.; Wang, C.; Hao, W.; Zhang, J. Photocatalytic Properties of BiOX (X = Cl, Br, and I). *Rare Metals* **2008**, *27*, 243-250.

(12) Jiang, J.; Zhao, K.; Xiao, X.; Zhang, L. Synthesis and Facet-Dependent Photoreactivity of BiOCl Single-Crystalline Nanosheets. *J. Am. Chem. Soc.* **2012**, *134*, 4473-4476.

(13) Shang, M.; Wang, W.; Zhang, L. Preparation of BiOBr Lamellar Structure with High Photocatalytic Activity by CTAB as Br Source and Template. *J. Hazard. Mater.* **2009**, *167*, 803-

809.

(14) Li, H.; Liu, J.; Liang, X.; Hou, W.; Tao, X. Enhanced Visible Light Photocatalytic Activity of Bismuth Oxybromide Lamellas with Decreasing Lamella Thicknesses. *J. Mater. Chem. A* **2014**, *2*, 8926-8932.

(15) Feng, J.; Qian, X.; Huang, C.-W.; Li, J. Strain-engineered Artificial Atom as a Broad-spectrum Solar Energy Funnel. *Nat. Photonics* **2012**, *6*, 866-872.

(16) Hÿtch, M. J.; Snoeck, E.; Kilaas, R. Quantitative Measurement of Displacement and Strain Fields from HREM Micrographs. *Ultramicroscopy* **1998**, *74*, 131-146.

(17) Grillo, V.; Rotunno, E. STEM_CELL: a Software Tool for Electron Microscopy: Part I-Simulations. *Ultramicroscopy* **2013**, *125*, 97-111.

(18) Grillo, V.; Rossi, F. STEM_CELL: a Software Tool for Electron Microscopy. Part 2 Analysis of Crystalline Materials. *Ultramicroscopy* **2013**, 112-129.

(19) Kresse, G.; Hafner, J. Ab Initio Molecular Dynamics for Open-shell Transition Metals. *Phys. Rev. B* **1993**, *48*, 13115-11318.

(20) Perdew, J. P.; Burke, K.; Ernzerhof, M. Generalized Gradient Approximation Made Simple. *Phys. Rev. Lett.* **1996**, *77*, 3865-3868.

(21) Blöchl, P. E. Projector Augmented-wave Method. *Phys. Rev. B* **1994**, *50*, 17953-17979.

(22) Shiri, D.; Kong, Y.; Buin, A.; Anantram, M. P. Strain Induced Changes of Bandgap and Effective Mass in Silicon Nanowires. *Appl. Phys. Lett.* **2008**, *93*, 073114.

(23) Li, W.; Wang, X.; Wang, Y.; Zhang, J.; Lin, Z.; Zhang, B.; Huang, F. Synthesis and Facet-Dependent Photocatalytic Activity of BiOBr Single-Crystalline Nanosheets. *Chem. Comm.* **2014**, DOI: 10.1039/C3CC41498A.

(24) Chen, J.; Guan, M.; Cai, W.; Guo, J.; Xiao, C.; Zhang, G. The Dominant {001} Facet-

dependent Enhanced Visible-light Photoactivity of Ultrathin BiOBr nanosheets. *Phys. Chem. Chem. Phys.* **2014**, *16*, 20909-20914.

Figures and figure captions

Figure 1

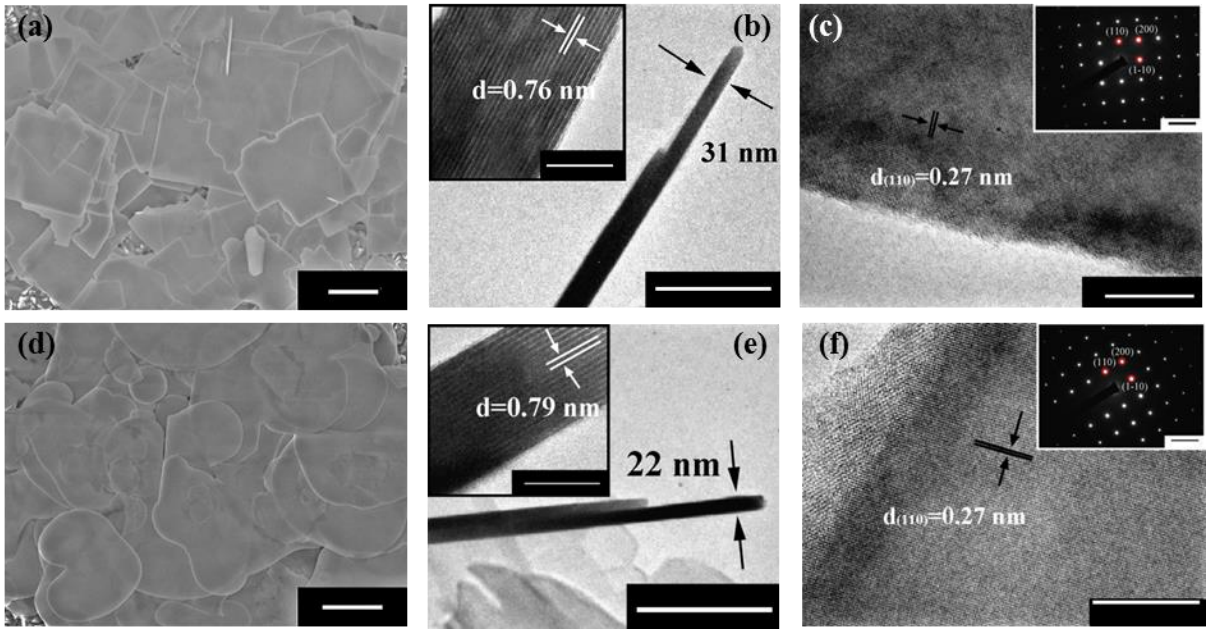

Figure 1. SEM images of (a) BiOBr-square and (d) BiOBr-circle (scale bar is 1 μm). Cross-sectional TEM images of (b) BiOBr-square and (e) BiOBr-circle (scale bar is 200 nm); insets are the HRTEM images of the cross-sections, where both samples show layer structure along the *c*-axis (scale bar is 10 nm). HRTEM images of (c) BiOBr-square and (f) BiOBr-circle, with the corresponding SAED patterns as the insets, indicating that both samples have the (001) face exposed (scale bar is 10 nm and 5 nm^{-1} for the insets).

Figure 2

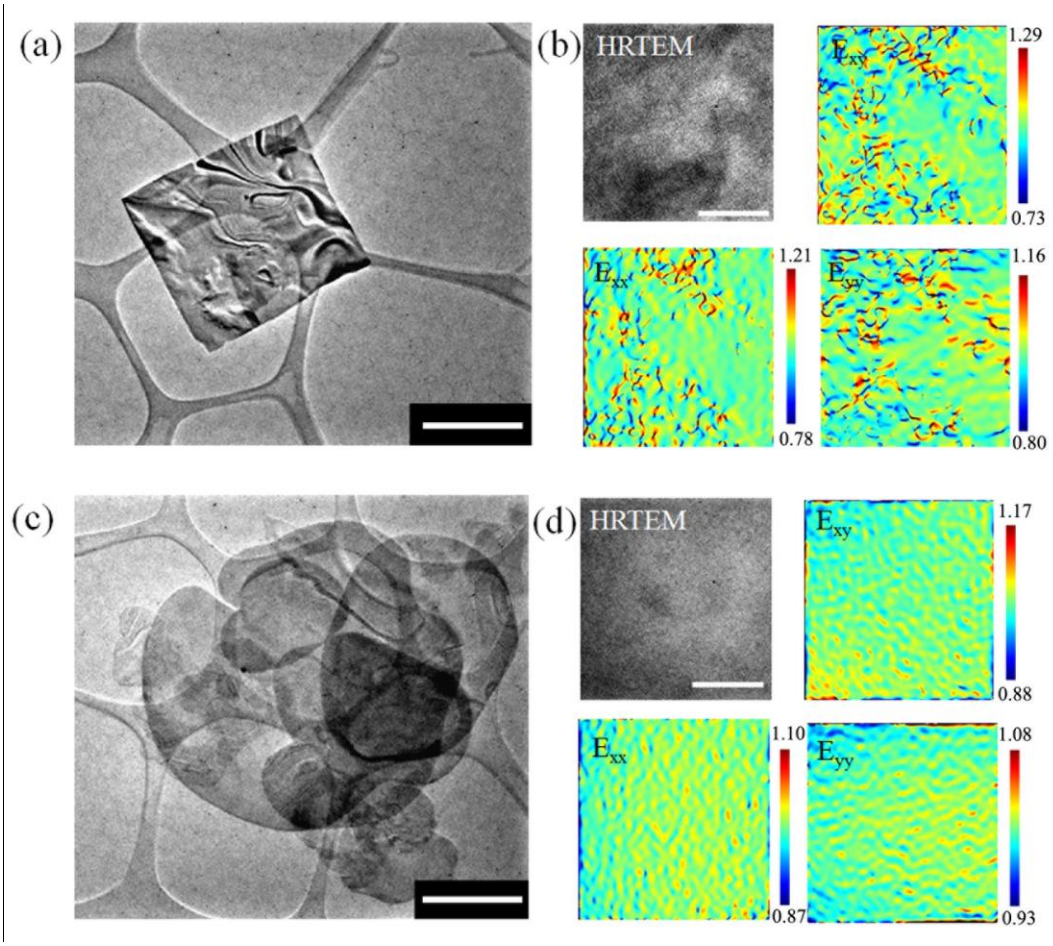

Figure 2. TEM images of (a) BiOBr-square and (c) BiOBr-circle (scale bars are 1000 nm). Strain simulation of (b) BiOBr-square and (d) BiOBr-circle based on HRTEM (scale bars are 10 nm). The internal strain distributions are in the xy-direction (E_{xy}), the x-direction (E_{xx}) and the y-direction (E_{yy}), with the scale for the whole image area.

Figure 3

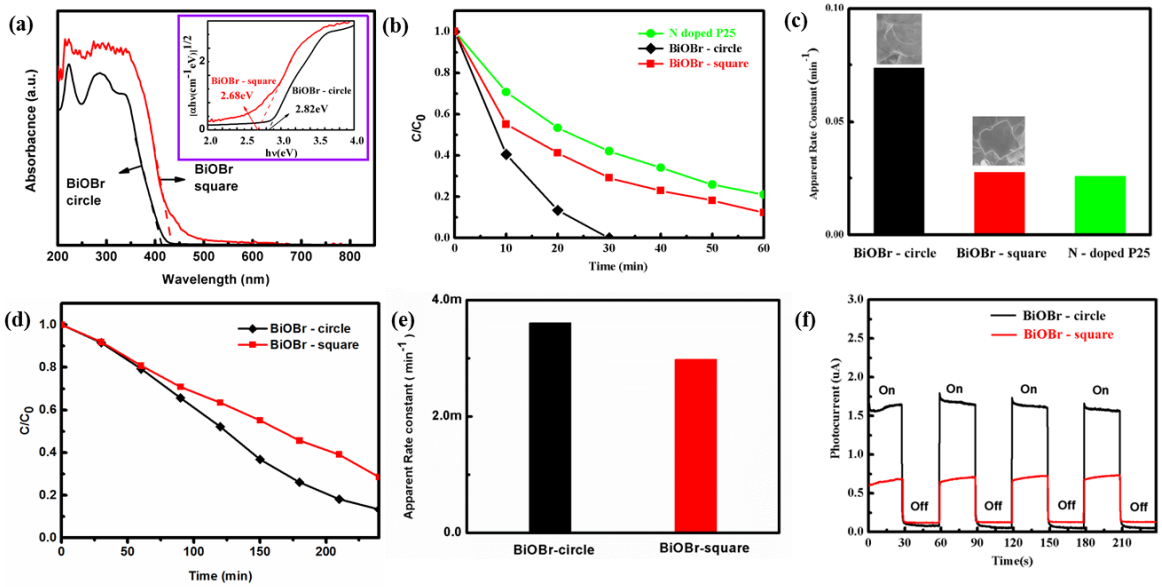

Figure 3. (a) UV-Vis diffuse reflectance spectra of BiOBr-square and BiOBr-circle; inset shows the derivation of the band-gap values for BiOBr. (b) Degradation experiments on Rh. B by P25, BiOBr-square, and BiOBr-circle under visible light irradiation, and (c) the corresponding apparent rate constants. (d) Degradation experiments on MO by BiOBr-square and BiOBr-circle under visible light irradiation, and (e) the corresponding apparent rate constants. (f) Current density transient with light on/off for BiOBr powders under light irradiation.

Figure 4

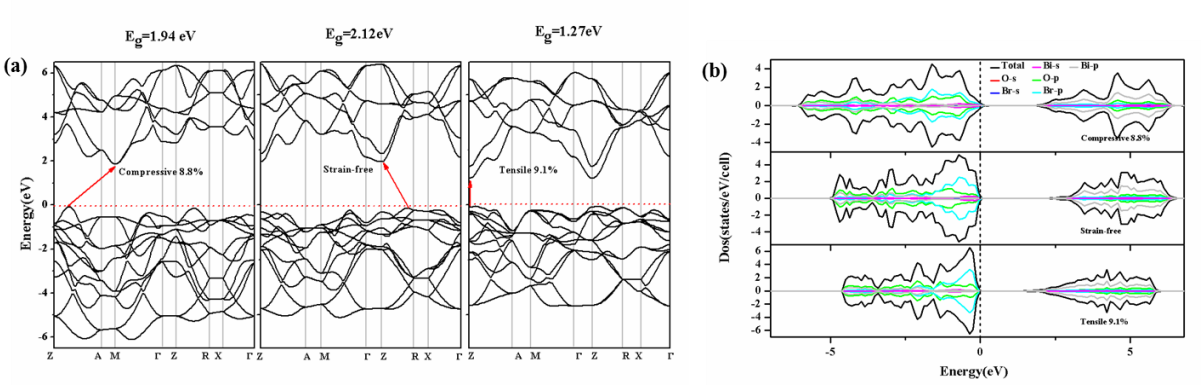

Figure 4. DFT calculations of the band structure of BiOBr with biaxial strain. (a) The left panel models compressive strain, the central panel is for a strain-free sample, and the right is for tensile strain. (b) Calculations of the DOS of BiOBr with different kinds of strain.

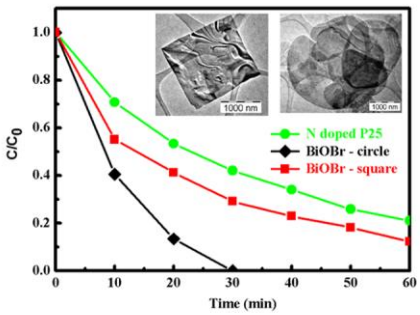

For Table of Contents Only